Operation of the voltage sensor of a human voltage- and Ca^{2+}-activated K^+ channel

Antonios Pantazis[a], Vadym Gudzenko[a], Nicoletta Savalli[a], Daniel Sigg[a], and Riccardo Olcese[a,b,c,1]

[a]Department of Anesthesiology, Division of Molecular Medicine, [b]Brain Research Institute, and [c]Cardiovascular Research Laboratory, David Geffen School of Medicine, University of California, Los Angeles, CA 90095-7115

Edited by Ramón Latorre, Centro de Neurociencias, Universidad de Valparaíso, Valparaíso, Chile, and approved January 7, 2010 (received for review October 23, 2009)

Voltage sensor domains (VSDs) are structurally and functionally conserved protein modules that consist of four transmembrane segments (S1–S4) and confer voltage sensitivity to many ion channels. Depolarization is sensed by VSD-charged residues residing in the membrane field, inducing VSD activation that facilitates channel gating. S4 is typically thought to be the principal functional component of the VSD because it carries, in most channels, a large portion of the VSD gating charge. The VSDs of large-conductance, voltage- and Ca^{2+}-activated K^+ channels are peculiar in that more gating charge is carried by transmembrane segments other than S4. Considering its "decentralized" distribution of voltage-sensing residues, we probed the BK_{Ca} VSD for evidence of cooperativity between charge-carrying segments S2 and S4. We achieved this by optically tracking their activation by using voltage clamp fluorometry, in channels with intact voltage sensors and charge-neutralized mutants. The results from these experiments indicate that S2 and S4 possess distinct voltage dependence, but functionally interact, such that the effective valence of one segment is affected by charge neutralization in the other. Statistical-mechanical modeling of the experimental findings using allosteric interactions demonstrates two mechanisms (mechanical coupling and dynamic focusing of the membrane electric field) that are compatible with the observed cross-segment effects of charge neutralization.

BK | cooperativity | fluorometry | Slo1 | MaxiK

BK_{Ca} channels (also known as MaxiK) are membrane proteins expressed in most mammalian cells (1). Their activation, by membrane potential depolarization or intracellular $[Ca^{2+}]$ increase (1–9) results in an exceptionally high conductance for K^+. As such, they are potent regulators of diverse cellular processes, including smooth muscle tone, neuronal excitability, and neurotransmitter release (8). Four pore-forming α subunits (10), encoded by KCNMA1 (*hSlo1*) in humans (11), are required to assemble into a functional channel. Each α subunit possesses an extracellular N terminus (12), seven transmembrane segments (S0–S6), and a large intracellular C-terminal region organized into domains RCK1 and RCK2 (Regulator of Conductance for K^+, Fig. 1*A*) that confer sensitivity to Ca^{2+} and other intracellular ligands (8, 9, 13–20). Segments S1–S6 are structurally and functionally homologous to those of other voltage-gated ion channels (21), with S1–S4 comprising the VSD, whereas S5 and S6 contribute to the K^+-selective pore.

Our understanding of VSD structure and function has been achieved thus far through analysis of crystal structures (22–24) as well as accessibility, electrophysiological, and optical investigations in functional proteins (reviewed in ref. 25). VSDs possess a high density of charged residues (Fig. 1*C*). Upon membrane potential depolarization, a subset of these residues may traverse the field partially or entirely, initiating conformational rearrangements that propagate to the channel gate, facilitating ionic conductance (26–28). S4 is thought to be the principal voltage-sensing segment because, in most VSD-gated channels, it contributes the greatest portion of gating charge movement (29–31). S2 usually carries less charge, but it can influence VSD activation by forming state-specific electrostatic interactions with S4 (32–36). Another important feature for VSD operation is the focusing of the electric field by water-filled crevices that can extend into the VSD core from either side of the cell membrane (37–43), effectively increasing gating charge movement and resulting in improved voltage sensitivity.

Recently, extensive electrophysiological analysis of the role of charged VSD residues in BK_{Ca} voltage-dependent activation (44) revealed that only one residue in the BK_{Ca} S4 senses voltage (R213) and that a greater portion of the total gating charge movement is contributed by residues outside this segment: one in S3 (D186) and two in S2 (D153, R167) (Fig. 1*B*). In light of this information, we optically tracked the voltage-dependent transitions of S2 and S4 in the human BK_{Ca}, by combining the cut-open oocyte Vaseline gap (COVG) voltage clamp technique (45) with site-specific tetra-methyl-rhodamine maleimide (TMRM) labeling and fluorometry (46–50). To probe for interactions between S2 and S4, we introduced charge-neutralizing mutations in either segment and tracked the activation of the other. We discovered that gating charge neutralization in one segment impaired the voltage dependence of the other and vice versa, demonstrating that S2 and S4 are functionally coupled. Based on the statistical-mechanical analysis of voltage-dependent BK_{Ca} activation, we propose two different, but not mutually exclusive, mechanistic interpretations of the cooperative coupling between S2 and S4: a special manifestation of mechanical coupling and dynamic (activation-dependent) focusing of the membrane electric field.

Results

Voltage-Dependent Conformational Changes Reported from the S2 BK_{Ca} Domain. Having characterized the voltage-dependent rearrangements of S4 (51, 52), we sought to resolve those of S2, which contains residues that make a significant contribution to BK_{Ca} gating charge displacement (44). Fig. 2*A* and *B* shows K^+ currents and TMRM fluorescence deflections ($\Delta F/F$), implying conformational rearrangements, simultaneously recorded from BK_{Ca} channels labeled at the extracellular tip of S2 (position 145).

The fitting of ionic conductance and $\Delta F/F$ isotherms with a Boltzmann distribution (see *SI Text*) for S2- and S4-labeled channels (Fig. 2 *C* and *F*) provides information on the voltage dependence of ionic conductance and VSD segment motions. The voltage-dependent movements of S2 exhibited a half-activation potential (V_{half}) of approximately −58 mV and effective charge (z) of 0.57 e^0. The conformational rearrangements of S4 (Fig. 2*E*) had a V_{half} of −79 mV and a z of 0.79 e^0 (Fig. 2*F*), similar to previously published measurements (51). The measured time-course of their activation was 5–6 ms (Fig. 2*E*), an

Author contributions: A.P., V.G., N.S., D.S., and R.O. designed research; A.P., V.G., N.S., and R.O. performed research; D.S. contributed new reagents/analytic tools; A.P., V.G., N.S., D.S., and R.O. analyzed data; and A.P., D.S., and R.O. wrote the paper.

The authors declare no conflict of interest.

This article is a PNAS Direct Submission.

[1]To whom correspondence should be addressed. E-mail: rolcese@ucla.edu.

This article contains supporting information online at www.pnas.org/cgi/content/full/0911959107/DCSupplemental.

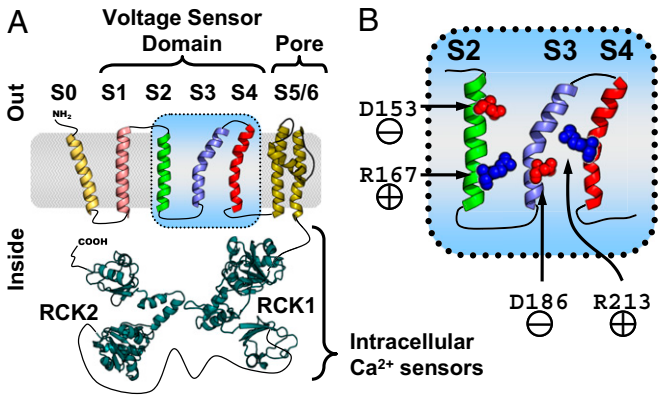

Fig. 1. BK_{Ca} α subunit topology and voltage-sensing residues. (*A*) BK_{Ca} channel α subunit membrane topology (12) and putative structure (intracellular Ca^{2+} sensing RCK1 and RCK2 by homology to a bacterial RCK domain (19). (*B*) Close-up of the BK_{Ca} voltage sensor domain (VSD) segments S2–S4, indicating the approximate positions of voltage-sensing residues D153 (S2) and D186 (S3) in red and R167 (S2) and R213 (S4) in blue (44).

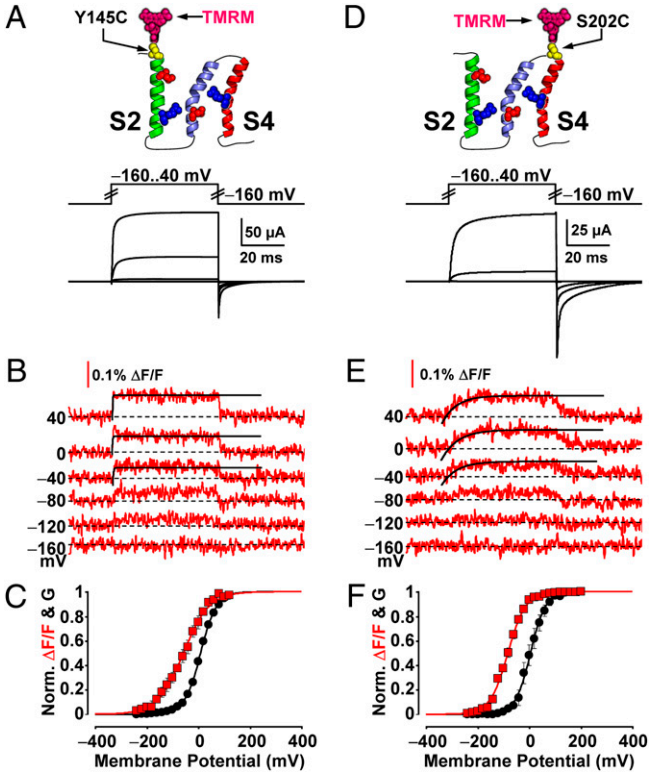

Fig. 2. Voltage-dependent structural transitions and ionic conductance from S2- and S4-labeled channels. (*A*) Voltage pulses and characteristic evoked K^+ currents from BK_{Ca} channels labeled with TMRM at position 145 (outside S2). (*B*) TMRM fluorescence traces recorded during the voltage pulses in *A*. Fitted activation exponentials (black) are τ = 0.130 μs for the 40 mV pulse, 220 μs for 0 mV, 300 μs for −40 mV. (*C*) Normalized K^+ conductance (G, black circles) and Δ*F*/*F* (red squares) plotted against membrane potential and fitted with Boltzmann distributions (black and red curves, respectively; see *SI Text*). Boltzmann parameters: G-V V_{half} = 9.9 ± 2.2 mV; z = 0.86 ± 0.1 e^0. F-V V_{half} = −58 ± 9.3 mV; z = 0.57 ± 0.05 e^0. n = 8 cells. (*D–F*) As in *A–C*, for channels labeled with TMRM at position 202, in the short extracellular linker between S3 and S4. Fitted activation exponentials in *E* (black) are τ = 5.2 ms for the 40 mV pulse, 6.1 ms for 0 mV, 6.0 ms for −40 mV. Boltzmann parameters in *F*: G-V (black) V_{half} = −1.0 ± 9.0 mV; z = 1.0 ± 0.053 e^0. F-V (red) V_{half} = −79 ± 4.2 mV; z = 0.79 ± 0.055 e^0. n = 7.

order of magnitude slower than those of S2 Δ*F*/*F* (130-300 μs, Fig. 2*B*). The difference in the voltage dependence of S2 and S4—also encountered in channels with neutralized voltage-sensing charges—and kinetics strongly supports that the reported TMRM fluorescence deflections were segment-specific.

Neutralizing Voltage-Sensing Residues Impairs the Voltage-Dependent Transitions of Their Segment. As the neutralization of charged residues D153 (S2) and R213 (S4) significantly decreased BK_{Ca} gating charge movement (44), neutralizing these residues should perturb the voltage dependence of the transmembrane segments bearing them. D153 was mutated to the uncharged residue glutamine in a BK_{Ca} clone with a TMRM label at the extracellular tip of S2. Macroscopic K^+ currents from these channels were only observed at extremely depolarized potentials, typically above 180 mV (Fig. 3*A*). Brief (10 ms) depolarizations up to 300 mV elicited outward K^+ current up to 200 μA, unlike in mock-injected oocytes (≈6 μA at 300 mV). The resolved Δ*F*/*F* (Fig. 3*B*) had extremely shallow voltage dependence, barely exhibiting saturation within the range of testable membrane potential (±300 mV, Fig. 3*C*). The maximum effective charge this data could be fitted with was 0.16 e^0. This marked loss of valence (>78%) is compatible with the prominent role of D153 in the voltage dependence of BK_{Ca} channel activation. The residual voltage dependence likely arose from another gating charge in S2, R167 (44).

Channels with a neutralized voltage-sensing charge in S4 (R213G) also required extremely depolarized potentials to exhibit macroscopic K^+ conductance (Fig. 3*D*). The voltage dependence of Δ*F*/*F* observed from position 202, at the short extracellular S3–S4 linker, differed from those of channels with an intact S4 in two ways: (*i*) it exhibited a reduction in effective charge by 70% and (*ii*) was shifted by 160 mV toward depolarized potentials (Fig. 3 *E* and *F*). Sequence homology (Fig. 1*C*), hydropathy analysis (12), and NMR spectroscopy (53) suggest that the extracellular linker between S3 and S4 in BK_{Ca} is only three residues long. Thus, the voltage-evoked movements of S3, which bears the voltage-sensing D186 (44), could contribute to the fluorescence deflections reported from position 202.

Charge Neutralization in S4 Impairs the Voltage Dependence of the Motion of S2 and Vice Versa. Although intrasubunit interactions between S2 and S4 have been reported in other voltage-gated channels (32–36), they have not been investigated using a segment-specific optical technique. To probe for such interactions within the BK_{Ca} VSD, we engineered channels with voltage-sensing charge neutralization in one segment and optically tracked the activation of the other. We first tracked the activation of S2 in channels bearing a charge-neutralizing mutation in S4, R213G. As in S4-labeled R213G clones (Fig. 3*D*), these channels required extremely depolarized potential to produce significant macroscopic K^+ current (Fig. 4*A*). S2 conformational transitions were reported by TMRM labeling position 145 (Fig. 4*B*). Their voltage dependence (Fig. 4*C*) was distinctly shallower than that from S2-labeled channels with an intact S4 (a reduction by 0.33 e^0). Similarly, a loss of 0.56 e^0 was exhibited by the Δ*F*/*F* of S4-labeled, S2-neutralized (D153Q) channels (Fig. 4 *D–F*). These experiments directly demonstrate that when one voltage-sensing segment is impaired (S2 or S4), the function of the neighboring segment is reciprocally affected supporting the hypothesis that the two voltage-sensing segments are functionally coupled.

The BK_{Ca} VSD Is Not a Rigid Structure. To explore the nature of the interaction between S2 and S4, we constructed statistical-mechanical models of voltage-dependent BK_{Ca} activation. The complete expressions for the energetic terms underlying these

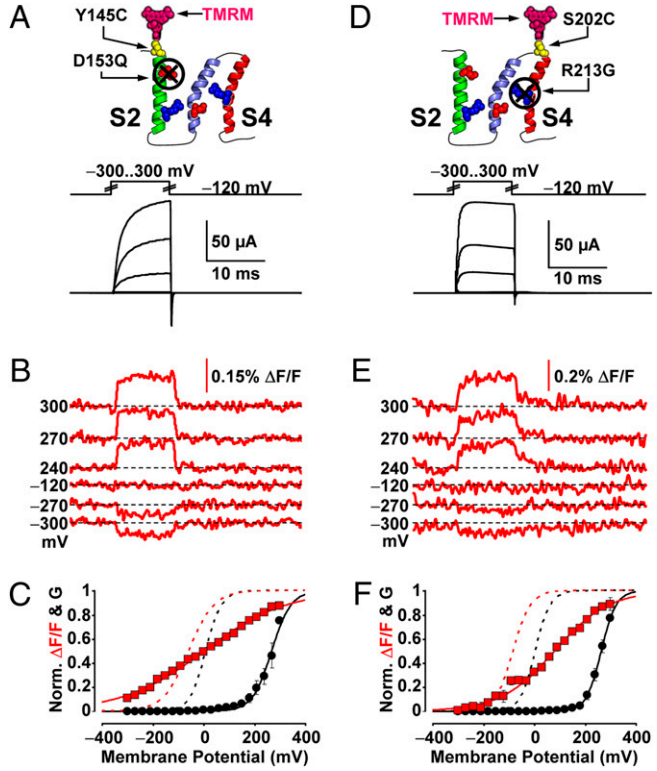

Fig. 3. Voltage-sensing charge neutralization impairs the voltage dependence of its segment. (*A*) Voltage pulses and characteristic evoked K^+ currents from BK_{Ca} channels labeled with TMRM at position 145 (outside S2) with mutation D153Q, to neutralize the voltage-sensing Aspartate of S2 (44). (*B*) TMRM fluorescence traces recorded during the voltage pulses in *A*. (*C*) Normalized K^+ conductance (G, black circles) and $\Delta F/F$ (red squares) plotted against membrane potential and fitted with Boltzmann distributions (black and red curves, respectively; see *SI Text*). Boltzmann parameters: G-V V_{half} = 285 ± 15 mV; z = 0.50 ± 0.03 e^0. F-V V_{half} = 3 ± 0.4 mV; z = 0.16 ± 0.001 e^0. n = 4 cells. G-V and F-V curves of the same clone without charge mutation are also included (dashed black and red curves, respectively). (*D–F*) As in *A–C*, for channels labeled with TMRM at position 202 (outside S4) with mutation R213G, to neutralize the single voltage-sensing residue of S4 (44). Boltzmann parameters in *F* are G-V V_{half} = 260 ± 5.7 mV; z = 0.89 ± 0.077 e^0. F-V V_{half} = 80 ± 2.2 mV; z = 0.24 ± 0.01 e^0. n = 7.

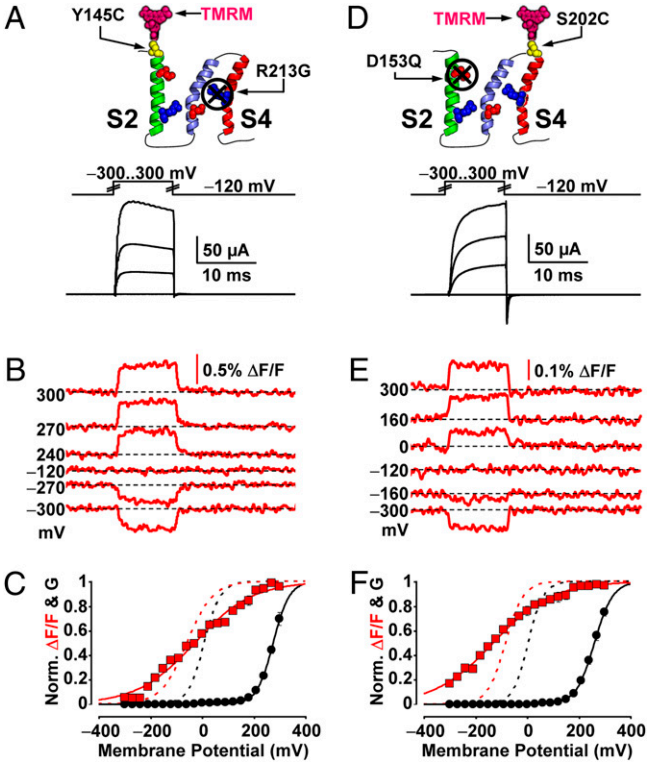

Fig. 4. Probing for evidence of S2–S4 interaction in the BK_{Ca} voltage sensor. (*A*) Voltage pulses and characteristic evoked K^+ currents from BK_{Ca} channels labeled with TMRM at position 145 (outside S2) with mutation R213G, to neutralize the single voltage-sensing residue of S4 (44). (*B*) TMRM fluorescence traces recorded during the voltage pulses in *A*. (*C*) Normalized K^+ conductance (G, black circles) and ΔF/F (red squares) plotted against membrane potential and fitted with Boltzmann distributions (black and red curves, respectively; see *SI Text*). Boltzmann parameters: G-V V_{half} = 277 ± 6 mV; z = 0.84 ± 0.01 e^0. F-V V_{half} = −28 ± 2 mV; z = 0.24 ± 0.01 e^0. n = 5 cells. G-V and F-V curves of the same clone without charge mutation are also included (dashed black and red curves, respectively). (*D–F*) As in *A–C*, for channels labeled with TMRM at position 202 (outside S4) with mutation D153Q, to neutralize the voltage-sensing Aspartate of S2 (44). Boltzmann parameters in *F* are: G-V V_{half} = 260 ± 5.6 mV; z = 0.74 ± 0.041 e^0. F-V V_{half} = −130 ± 1.8 mV; z = 0.23 ± 0.018 e^0. n = 5.

models, and the fitting regime, are in *SI Text*. The first tested premise is that the voltage sensor operates as a single functional unit, whereby transmembrane segments comprise a rigid structure possessing uniform voltage dependence. In this context, neutralization of a voltage-sensing residue anywhere in the VSD would produce a global reduction in effective charge. This model possesses four voltage-sensing domains energetically linked to the pore (Fig. S1*A*, scheme I). As this model produces the same voltage dependence of activation for S2 and S4, it is unable to reproduce the experimental data, whereby S2 and S4 exhibit distinct voltage dependence (Fig. S1 *B–D*). This result confirmed that the $\Delta F/F$ reported from S2 and S4 did not reflect the same voltage-dependent process, supporting our premise that the resolved conformational rearrangements are segment-specific.

A State-Dependent Interaction Alone Is Unable to Account for S2–S4 Cooperativity. To account for the difference in the voltage dependence of activation exhibited by S2 and S4, the VSD was separated into two subdomains, S2 and S4, with distinct voltage dependence (Fig. 5*A*, scheme II). Their activation is mutually facilitated by cooperative energetic interaction H_{24}, which lowers the free energy of the doubly activated VSD state. H_{24} is compatible with an electrostatic coupling between S2 and S4, such as was demonstrated in *Shaker* (32–34) and HERG (35, 36) K^+ channels, but could also represent steric, hydrophobic, or other state-specific interactions. This model can produce distinct activation curves for S2 and S4 and predicts data from channels without charge mutations well (Fig. 5*B*). However, it cannot account for the reduction in the effective charge of labeled segments when a charge in the neighboring segment is neutralized, instead producing steep activation curves (Fig. 5 *C* and *D*). This result indicates that a different basis of interaction, more directly related to segment valence, is required. Because of the extremely shallow S2 F-V curve from S2-neutralized (D153Q) channels (lacking evident saturation within the tested membrane potential range of ±300 mV, Fig. 3*B*), the experimental data (Fig. 5*C*, blue diamonds) were normalized to the prediction of the models but were not included in the simultaneous curve fitting.

A Model of Reciprocal Mechanical Coupling Between S2 and S4 Can Account for Their Activation. A central assumption of the (unsuccessful) scheme II (Fig. 5 *A–E*) is that S2 and S4 activate with effective charge q_{S2} and q_{S4}, respectively, without perturbing each other's charge movement during activation. However, the two segments could mechanically interact, or "nudge" each other, during their activation pathway through the membrane field. To

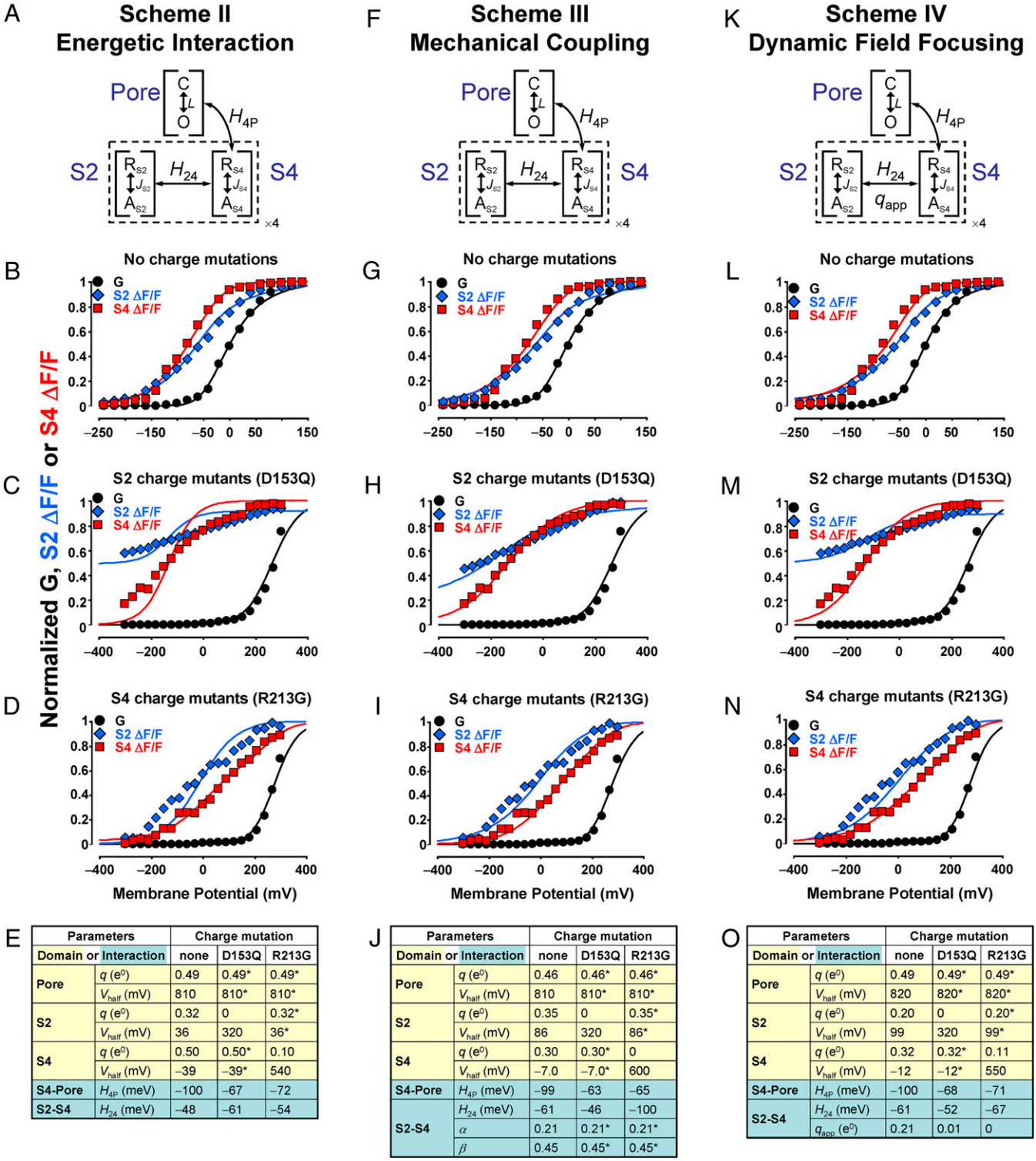

Parameters		Charge mutation		
Domain or Interaction		none	D153Q	R213G
Pore	q (e^0)	0.49	0.49*	0.49*
	V_{half} (mV)	810	810*	810*
S2	q (e^0)	0.32	0	0.32*
	V_{half} (mV)	36	320	36*
S4	q (e^0)	0.50	0.50*	0.10
	V_{half} (mV)	−39	−39*	540
S4-Pore	H_{4P} (meV)	−100	−67	−72
S2-S4	H_{24} (meV)	−48	−61	−54

Parameters		Charge mutation		
Domain or Interaction		none	D153Q	R213G
Pore	q (e^0)	0.46	0.46*	0.46*
	V_{half} (mV)	810	810*	810*
S2	q (e^0)	0.35	0	0.35*
	V_{half} (mV)	86	320	86*
S4	q (e^0)	0.30	0.30*	0
	V_{half} (mV)	−7.0	−7.0*	600
S4-Pore	H_{4P} (meV)	−99	−63	−65
S2-S4	H_{24} (meV)	−61	−46	−100
	α	0.21	0.21*	0.21*
	β	0.45	0.45*	0.45*

Parameters		Charge mutation		
Domain or Interaction		none	D153Q	R213G
Pore	q (e^0)	0.49	0.49*	0.49*
	V_{half} (mV)	820	820*	820*
S2	q (e^0)	0.20	0	0.20*
	V_{half} (mV)	99	320	99*
S4	q (e^0)	0.32	0.32*	0.11
	V_{half} (mV)	−12	−12*	550
S4-Pore	H_{4P} (meV)	−100	−68	−71
S2-S4	H_{24} (meV)	−61	−52	−67
	q_{app} (e^0)	0.21	0.01	0

Fig. 5. Allosteric models of voltage-dependent BK_{Ca} activation. (*A*) scheme II: Each BK_{Ca} VSD (dashed line) is separated into subdomains S2 and S4 with distinct voltage dependence, linked by activation-dependent, intrasubunit interaction H_{24}. The Pore domain can assume the closed (C) or open (O) state, whereas S2 and S4 can be either resting (R) or active (A). S4 activation stabilizes Pore opening via interaction H_{4P}. (*B*) Normalized K^+ conductance (G, black circles), S2 Δ*F*/*F* (blue diamonds), and S4 Δ*F*/*F* (red squares) from channels without charge neutralization (Fig. 2). scheme II predictions for conductance, S2 and S4 activation are shown as black, blue, and red curves, respectively. (*C*) As in *B* for channels with mutation D153Q in S2 (Figs. 3 *A*–*C* and 4 *D*–*F*). The highly linear S2 Δ*F*/*F* data (see Fig. 3*B*) were renormalized to conform to the model prediction, instead of constraining it. (*D*) As in *B*, for channels with mutation R213G in S4 (Figs. 3 *D*–*F* and 4 *A*–*C*). (*E*) scheme II fitted parameters. Parameters of charge-neutralized channels with an asterisk were constrained to be equal to their pseudo-WT channel equivalent. (*F*) scheme III. This model is similar to II, but predicts that a segment displaces its neighbor during activation, producing a fractional movement of its charge through the membrane field (see Fig. 6*A*). (*G*–*J*) As in *B*–*E*, for scheme III. (*K*) scheme IV is based on scheme II, with the addition of a voltage- and activation-dependent interaction q_{app} (see Fig. 6*B*). (*L*–*O*) As in *B*–*E*, for scheme IV.

test this condition, we constructed scheme III (Fig. 5 *F–J*), whereby activation of S2 causes a fractional charge movement in S4, while itself experiencing a reactionary force that limits the full extent of charge movement in its own segment. Thus, the charge moved by S2 activation is $(1-\beta)q_{S2}+\alpha q_{S4}$, where αq_{S4} and βq_{S2} are fractional charges of S4 and S2, respectively. Similarly, S4 activation displaces charge $(1-\alpha)q_{S4}+\beta q_{S2}$. According to the best fitting (Fig. 5*J*), the fraction of S4 charge movement during S2 activation (α) is 0.21, whereas the equivalent value for S2 (β) is 0.45. S4 activation in the WT effectively moves 0.39 e^0, in S2-neutralized channels (D135Q) 0.24 e^0, and in S4-neutralized channels (R213G) 0.16 e^0. S2 activation in the WT effectively moves 0.26 e^0, in S2-neutralized channels 0.06 e^0, and in S4 neutralized channels 0.19 e^0. As in scheme I, the total charge moved by S2 and S4 activation is $q_{S2}+q_{S4}$. However, this model allows for the apparent reduction of charge in a segment when its neighbor is neutralized, so it can predict the data satisfactorily (Fig. 5 *G–I*), making a reciprocal mechanical perturbation during S2/S4 activation a plausible explanation.

An Alternative Model Involving a Voltage-Dependent Mode of Cooperativity. A different mechanism (Fig. 5*K*, scheme IV) can account for the experimental findings, in which additional charge is moved in the S2/S4 doubly activated state (q_{app}), resulting in a de facto voltage-dependent cooperative interaction. This model predicts a steeper voltage dependence experienced by S2 or S4 upon activation of the other sensor (Fig. 5 *L–N*) and is consistent with a dynamic field focusing interpretation discussed further on. The voltage-independent term H_{24} is of considerable magnitude (−61 meV, equivalent to 2.4 kT or coupling factor 11) and is little affected by charge neutralization. Conversely, charge neutralization in a segment not only decreases its own charge but also reduces q_{app} from 0.21 e^0 to almost zero, resulting in the reduced voltage dependence of the neighboring, intact segment (Fig. 5 *M* and *N*), as observed experimentally (Fig. 4). When direct comparison of parameters can be made, the fitting of scheme IV is in congruence with the findings of a previous model of BK_{Ca} activation (44). Specifically, the Pore Domain voltage dependence (L_0 equivalent to V_{half} = 818 mV at 25 °C, z_L = 0.49 e^0; scheme IV: V_{half} = 820 mV, q = 0.49 e^0) and the VSD-Pore interaction (factor D equivalent to −80 meV at 25 °C; scheme IV H_{4P}: −100 meV). Because q_{app} lowers the free energy of the doubly activated VSD, it is a cooperative element.

Discussion

We used voltage-clamp fluorometry to optically track the activation of gating-charge-bearing transmembrane domains S2 and S4 in the human BK_{Ca} VSD. These experiments showed that S2 and S4 possess distinct voltage dependence but also revealed that charge neutralization in one voltage-sensing segment reciprocally reduced the voltage dependence of its neighbor. This clearly indicated that S2 and S4 are functionally coupled, influencing each other's voltage-sensing ability. The possibility that activation of S2 could somewhat influence the fluorescence signal of S4 and vice versa (a condition referred to as signal cross-talk) has been investigated extensively both at the macroscopic domain and the microscopic level. The results of this analysis show that signal cross-talk cannot account for the experimental findings and, if cross-talk does occur, it does not significantly affect on our results and conclusions. The analysis can be found in *SI Text*, "Investigating signal cross-talk," and Figs. S2–S4.

To understand the nature of the intrasubunit interactions between S2 and S4, we formulated and tested statistical-mechanical models of voltage-dependent BK_{Ca} activation based on different premises. Models assuming that the BK_{Ca} VSD operates as a single unit with uniform voltage dependence (Fig. S1 *A–E*, scheme I) or on the basis of an energetic S2–S4 interaction alone (Fig. 5 *A–E*, scheme II) could not account for the data. One model that produced a satisfactory fit (Fig. 5 *F–J*, scheme III) was similar to scheme II, with the additional condition that S2 and S4 mechanically perturb each other during activation (Fig. 6*A*), such that when one segment is neutralized, the charge moved when its intact partner activates is reduced. A similar mechanism has been proposed to account for the weak voltage dependence of pore opening transitions in BK_{Ca}, whereby activating pore structures could displace VSD segments (4).

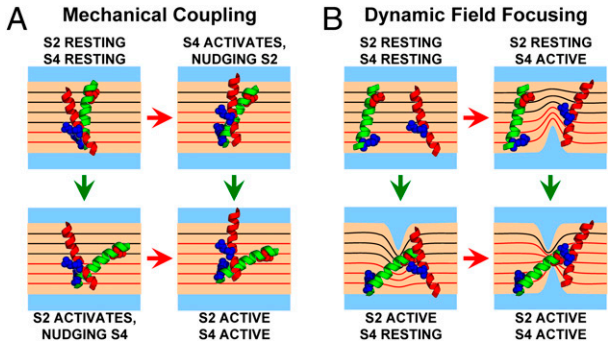

Fig. 6. The mechanical coupling and dynamic field focusing theories. S2 (green helix) and S4 (red helix) of a wild-type BK_{Ca} VSD undergo hypothetical motions during activation. Only segments from one subunit are shown for clarity, possessing voltage-sensing residues: D153 (S2, red), R167 (S2, blue) and R213 (S4, blue) (44). The membrane voltage drop is illustrated by equipotential lines (in black, except the portion traversed by R213 in S4, in red lines). (*A*) According to the mechanical coupling theory (Fig. 5 *F–J*, scheme III), segment activation causes the displacement, or nudging, of its neighbor, producing a fractional movement of its charge through the membrane field. (*B*) According to the dynamic field focusing theory, segment activation causes aqueous crevices to form, focusing the field. As a result, in the S2/S4 doubly activated state, these segments have traversed a large portion of the membrane potential, giving rise to q_{app}, fitted in scheme IV (Fig. 5 *K–O*).

Scheme IV also provides a plausible mechanism for the S2–S4 interaction while successfully predicting the data (Fig. 5 *K–O*). In this model, activation of S2 or S4 when the other segment has activated produces more charge movement than transitions to a single-activated state. This "non-additivity" of charge movement during activation is consistent with the dynamic (activation-dependent) electric field focusing illustrated in Fig. 6*B*, inspired by previous postulation in *Shaker* K^+ channels (43, 47): Activation of a voltage-sensing segment could modify aqueous crevices, focusing the field over a shorter dielectric distance. A charged, neighboring segment would then traverse a larger portion of the voltage drop across the membrane, so an observer would measure increased charge movement. Likewise, failure of a segment to focus the field results in loss of effective charge by its neighbor. Consequently, aqueous crevices could be a dynamic, activation-dependent element of the BK_{Ca} VSD, rather than a passive morphological feature. We find this interpretation more conceptually satisfying, because it is based on significant evidence supporting the existence of VSD crevices (37–43), including in BK_{Ca} (54).

Schemes II–IV assume that pore opening is facilitated by S4 activation via energetic interaction H_{4P}. Including a similar interaction between S2 and the pore (H_{2P}) mainly decreased the magnitude of H_{4P} without significantly affecting the rest of the parameters or the goodness of the fits (Fig. S1 *F–J*). A recent model of BK_{Ca} includes S2 as the most distal segment to pore structures (55), although investigations on KvAP channels suggest otherwise (42). Because we cannot distinguish between these alternative models, we can neither ascertain nor refute direct S2-dependent gating in BK_{Ca}.

We have demonstrated that transmembrane domains S2 and S4 in the human BK_{Ca} VSD possess distinct voltage dependence but also interact during activation. An interesting finding is that charge

movement in one segment is perturbed by charge neutralization in its neighbor. We propose two interpretations to account for the apparent S2–S4 interaction, which are not mutually exclusive: mechanical coupling (Fig. 6*A*) and dynamic field focusing (Fig. 6*B*). The VSD of human BK_{Ca} channels has been an ideal system to study such interactions because of its "decentralized" distribution of voltage-sensing residues throughout the VSD (Fig. 1*B* and S5) (44). Nevertheless, the charged residues neutralized in this investigation and VSD topology are highly conserved (Fig. S5), so it would be of prime interest to pursue the demonstration of similar interactions in other members of the voltage-activated protein superfamily.

Materials and Methods

All experiments were performed on human BK_{Ca} channel α subunit clones (*hSlo1*) (11) with these background mutations: (*i*) all native extracellular Cysteines were substituted to Serines (C14S, C141S, C277S); (*ii*) W203V, which increases the amplitude of voltage-dependent TMRM Δ*F*/*F* from position 202 outside S4 (51); and (*iii*) R207Q, to increase P_O at low intracellular [Ca^{2+}] (3, 51, 52) without influencing gating charge movement (44). Site-directed mutagenesis was performed with QuikChange (Stratagene) and confirmed by sequence analysis. The clones were transcribed in vitro (T7 mMessage mMachine; Ambion) for oocyte injection. *Xenopus laevis* (NASCO) oocytes (stage V–VI) were prepared, injected, and labeled with TMRM as described (51).

Ionic currents were recorded from oocytes under voltage clamp by using the COVG technique (45) in a set-up modified to allow epifluorescence measurements (49). External solution: 120 mM NaMES, 10 mM KMES, 2 mM $Ca(MES)_2$, and 10 mM HEPES. Internal solution: 110 mM K-Glutamate and 10 mM K-HEPES. Intracellular micropipette solution: 2.7 M NaMES and 10 mM NaCl. The holding V_m was −90 mV.

Please see *SI Text* for data analysis methods, the model construction and fitting routine.

ACKNOWLEDGMENTS. We thank Michela Ottolia and members of the R.O. laboratory for constructive discussion on the manuscript. The *hSlo1* clone was a kind gift from Ligia Toro. This work was supported by research grants from National Institutes of Health/National Institute of General Medical Sciences R01GM082289 and the Laubisch Foundation (R.O.), and an American Heart Association Postdoctoral Fellowship (Western States Affiliate) (to A.P.).

1. Salkoff L, Butler A, Ferreira G, Santi C, Wei A (2006) High-conductance potassium channels of the SLO family. *Nat Rev Neurosci* 7:921–931.
2. Stefani E, et al. (1997) Voltage-controlled gating in a large conductance Ca2+-sensitive K+channel (hslo). *Proc Natl Acad Sci USA* 94:5427–5431.
3. Díaz L, et al. (1998) Role of the S4 segment in a voltage-dependent calcium-sensitive potassium (hSlo) channel. *J Biol Chem* 273:32430–32436.
4. Horrigan FT, Cui J, Aldrich RW (1999) Allosteric voltage gating of potassium channels I. Mslo ionic currents in the absence of Ca(2+). *J Gen Physiol* 114:277–304.
5. Horrigan FT, Aldrich RW (1999) Allosteric voltage gating of potassium channels II. Mslo channel gating charge movement in the absence of Ca(2+). *J Gen Physiol* 114: 305–336.
6. Horrigan FT, Aldrich RW (2002) Coupling between voltage sensor activation, Ca2+ binding and channel opening in large conductance (BK) potassium channels. *J Gen Physiol* 120:267–305.
7. Magleby KL (2003) Gating mechanism of BK (Slo1) channels: So near, yet so far. *J Gen Physiol* 121:81–96.
8. Latorre R, Brauchi S (2006) Large conductance Ca2+-activated K+ (BK) channel: activation by Ca2+ and voltage. *Biol Res* 39:385–401.
9. Cui J, Yang H, Lee US (2009) Molecular mechanisms of BK channel activation. *Cell Mol Life Sci* 66:852–875.
10. Shen KZ, et al. (1994) Tetraethylammonium block of Slowpoke calcium-activated potassium channels expressed in Xenopus oocytes: Evidence for tetrameric channel formation. *Pflugers Arch* 426:440–445.
11. Wallner M, et al. (1995) Characterization of and modulation by a beta-subunit of a human maxi KCa channel cloned from myometrium. *Receptors Channels* 3:185–199.
12. Wallner M, Meera P, Toro L (1996) Determinant for beta-subunit regulation in high-conductance voltage-activated and Ca(2+)-sensitive K+ channels: an additional transmembrane region at the N terminus. *Proc Natl Acad Sci USA* 93:14922–14927.
13. Wei A, Solaro C, Lingle C, Salkoff L (1994) Calcium sensitivity of BK-type KCa channels determined by a separable domain. *Neuron* 13:671–681.
14. Jiang Y, Pico A, Cadene M, Chait BT, MacKinnon R (2001) Structure of the RCK domain from the E. coli K+ channel and demonstration of its presence in the human BK channel. *Neuron* 29:593–601.
15. Salkoff L (2006) A tail of multiple calcium-sensing domains. *J Gen Physiol* 128:387–388.
16. Lingle CJ (2007) Gating rings formed by RCK domains: Keys to gate opening. *J Gen Physiol* 129:101–107.
17. Sweet TB, Cox DH (2008) Measurements of the BKCa channel's high-affinity Ca2+ binding constants: Effects of membrane voltage. *J Gen Physiol* 132:491–505.
18. Yang H, et al. (2008) Activation of Slo1 BK channels by Mg2+ coordinated between the voltage sensor and RCK1 domains. *Nat Struct Mol Biol* 15:1152–1159.
19. Yusifov T, Savalli N, Gandhi CS, Ottolia M, Olcese R (2008) The RCK2 domain of the human BKCa channel is a calcium sensor. *Proc Natl Acad Sci USA* 105:376–381.
20. Hou S, Heinemann SH, Hoshi T (2009) Modulation of BKCa channel gating by endogenous signaling molecules. *Physiology (Bethesda)* 24:26–35.
21. Armstrong CM (2003) Voltage-gated K channels. *Sci STKE* 2003:re10.
22. Jiang Y, et al. (2003) X-ray structure of a voltage-dependent K+ channel. *Nature* 423: 33–41.
23. Long SB, Campbell EB, Mackinnon R (2005) Crystal structure of a mammalian voltage-dependent Shaker family K+ channel. *Science* 309:897–903.
24. Long SB, Tao X, Campbell EB, MacKinnon R (2007) Atomic structure of a voltage-dependent K+ channel in a lipid membrane-like environment. *Nature* 450:376–382.
25. Bezanilla F (2008) How membrane proteins sense voltage. *Nat Rev Mol Cell Biol* 9: 323–332.
26. Sigg D, Bezanilla F (1997) Total charge movement per channel. The relation between gating charge displacement and the voltage sensitivity of activation. *J Gen Physiol* 109:27–39.
27. Yellen G (1998) The moving parts of voltage-gated ion channels. *Q Rev Biophys* 31: 239–295.
28. Gagnon DG, Bezanilla F (2009) A single charged voltage sensor is capable of gating the Shaker K+ channel. *J Gen Physiol* 133:467–483.
29. Seoh SA, Sigg D, Papazian DM, Bezanilla F (1996) Voltage-sensing residues in the S2 and S4 segments of the Shaker K+ channel. *Neuron* 16:1159–1167.
30. Aggarwal SK, MacKinnon R (1996) Contribution of the S4 segment to gating charge in the Shaker K+ channel. *Neuron* 16:1169–1177.
31. Zhang M, Liu J, Tseng GN (2004) Gating charges in the activation and inactivation processes of the HERG channel. *J Gen Physiol* 124:703–718.
32. Papazian DM, et al. (1995) Electrostatic interactions of S4 voltage sensor in Shaker K+ channel. *Neuron* 14:1293–1301.
33. Tiwari-Woodruff SK, Lin MA, Schulteis CT, Papazian DM (2000) Voltage-dependent structural interactions in the Shaker K(+) channel. *J Gen Physiol* 115:123–138.
34. Silverman WR, Roux B, Papazian DM (2003) Structural basis of two-stage voltage-dependent activation in K+ channels. *Proc Natl Acad Sci USA* 100:2935–2940.
35. Zhang M, et al. (2005) Interactions between charged residues in the transmembrane segments of the voltage-sensing domain in the hERG channel. *J Membr Biol* 207:169–181.
36. Piper DR, Rupp J, Sachse FB, Sanguinetti MC, Tristani-Firouzi M (2008) Cooperative interactions between R531 and acidic residues in the voltage sensing module of hERG1 channels. *Cell Physiol Biochem* 21:37–46.
37. Starace DM, Stefani E, Bezanilla F (1997) Voltage-dependent proton transport by the voltage sensor of the Shaker K+ channel. *Neuron* 19:1319–1327.
38. Asamoah OK, Wuskell JP, Loew LM, Bezanilla F (2003) A fluorometric approach to local electric field measurements in a voltage-gated ion channel. *Neuron* 37:85–97.
39. Starace DM, Bezanilla F (2004) A proton pore in a potassium channel voltage sensor reveals a focused electric field. *Nature* 427:548–553.
40. Tombola F, Pathak MM, Isacoff EY (2005) Voltage-sensing arginines in a potassium channel permeate and occlude cation-selective pores. *Neuron* 45:379–388.
41. Ahern CA, Horn R (2005) Focused electric field across the voltage sensor of potassium channels. *Neuron* 48:25–29.
42. Chakrapani S, Cuello LG, Cortes DM, Perozo E (2008) Structural dynamics of an isolated voltage-sensor domain in a lipid bilayer. *Structure* 16:398–409.
43. Chanda B, Bezanilla F (2008) A common pathway for charge transport through voltage-sensing domains. *Neuron* 57:345–351.
44. Ma Z, Lou XJ, Horrigan FT (2006) Role of charged residues in the S1-S4 voltage sensor of BK channels. *J Gen Physiol* 127:309–328.
45. Stefani E, Bezanilla F (1998) Cut-open oocyte voltage-clamp technique. *Methods Enzymol* 293:300–318.
46. Mannuzzu LM, Moronne MM, Isacoff EY (1996) Direct physical measure of conformational rearrangement underlying potassium channel gating. *Science* 271:213–216.
47. Cha A, Bezanilla F (1997) Characterizing voltage-dependent conformational changes in the Shaker K+ channel with fluorescence. *Neuron* 19:1127–1140.
48. Gandhi CS, Isacoff EY (2005) Shedding light on membrane proteins. *Trends Neurosci* 28:472–479.
49. Gandhi CS, Olcese R (2008) *Methods in Molecular Biology, Potassium Channels*, ed Lippiat JD (Humana, Totowa, NJ), pp 213–231.
50. Horne AJ, Fedida D (2009) Use of voltage clamp fluorimetry in understanding potassium channel gating: a review of Shaker fluorescence data. *Can J Physiol Pharmacol* 87:411–418.
51. Savalli N, Kondratiev A, Toro L, Olcese R (2006) Voltage-dependent conformational changes in human Ca(2+)- and voltage-activated K(+) channel, revealed by voltage-clamp fluorometry. *Proc Natl Acad Sci USA* 103:12619–12624.
52. Savalli N, Kondratiev A, de Quintana SB, Toro L, Olcese R (2007) Modes of operation of the BKCa channel beta2 subunit. *J Gen Physiol* 130:117–131.
53. Unnerståle S, Lind J, Papadopoulos E, Mäler L (2009) Solution structure of the HsapBK K+ channel voltage-sensor paddle sequence. *Biochemistry* 48:5813–5821.
54. Hu L, et al. (2003) Participation of the S4 voltage sensor in the Mg2+-dependent activation of large conductance (BK) K+ channels. *Proc Natl Acad Sci USA* 100: 10488–10493.
55. Liu G, et al. (2008) Position and role of the BK channel alpha subunit S0 helix inferred from disulfide crosslinking. *J Gen Physiol* 131:537–548.